NANO LETTERS

pubs.acs.org/NanoLett

Unraveling Single-Stranded DNA in a Solid-State Nanopore

Stefan W. Kowalczyk, Maarten W. Tuijtel, Serge P. Donkers, and Cees Dekker*

Kavli Institute of Nanoscience, Delft University of Technology, Lorentzweg 1, 2628 CJ Delft, The Netherlands

ABSTRACT Solid-state nanopores are an emerging class of single-molecule sensors. Whereas most studies so far focused on double-stranded DNA (dsDNA) molecules, exploration of single-stranded DNA (ssDNA) is of great interest as well, for example to employ such a nanopore device to read out the sequence. Here, we study the translocation of long random-sequence ssDNA through nanopores. Using atomic force microscopy, we observe the ssDNA to hybridize into a random coil, forming blobs of around 100 nm in diameter for 7 kb ssDNA. These large entangled structures have to unravel, when they arrive at the pore entrance. Indeed, we observe strong blockade events with a translocation time that is exponentially dependent on voltage, $\tau \sim e^{-V/V_0}$. Interestingly, this is very different than for dsDNA, for which $\tau \sim 1/V$. We report translocations of ssDNA but also of ssDNA−dsDNA constructs where we compare the conductance-blockade levels for ssDNA versus dsDNA as a function of voltage.

KEYWORDS Nanopores, translocation, single-stranded DNA, sequencing

Solid-state nanopores[1,2] have proven to be an interesting new class of devices to characterize biopolymers such as DNA,[3,4] RNA,[5] as well as DNA/protein,[6,7] and DNA/ligand[8] complexes at the single-molecule level. The basic principle is simple: when a molecule is driven through a nanopore by an externally applied electric field, it causes a characteristic temporary change in the trans-pore current, allowing one to scan the molecule along its length. Both biological and solid-state nanopores have been proposed as candidates for sequencing applications.[9−11] While many beautiful single-molecule results have been reported for α-hemolysin,[12−16] the instability issues of the lipid bilayers in which these α-hemolysin pores are inserted, remain a challenge. Solid-state nanopores do not suffer from such instabilities and allow flexibility in pore size and shape. Here, we demonstrate, for the first time, the translocation of long random-sequence single-stranded DNA through solid-state nanopores at neutral pH. These ssDNA molecules hybridize in a complicated three-dimensional entangled structure through local hybridization at many hundreds of spots, or so-called nuclei, see for example ref 17. This yields a highly connected structure that needs to unravel to fit through the nanopore.

While many experiments on double-stranded molecules have been performed in solid-state nanopores, the single-stranded arena is much less explored. Double-stranded DNA that was denatured at very high pH (∼12) could be studied,[18] and recently single-stranded homopolymers poly(A), poly(U), and poly(C) were translocated through solid-state nanopores.[5] References 19 and 20 studied translocation of short ssDNA with a single hairpin. We take two approaches to address long heterosequence single-stranded DNA at neutral pH. First, we construct long single-stranded tails of different lengths on double-stranded DNA, using an Exonuclease III enzyme.[21,22] This enables us to study the pore entrance dynamics of single-stranded versus double-stranded DNA. We find that the double-stranded DNA enters the pore much more easily than the single-stranded DNA. Second, we study the translocation of the single-stranded viral DNA M13mp18 that was isolated from a phage vector, and we compare the results to those obtained with our hybrid ds/ss-molecules. Both types of molecules are also studied by atomic force microscopy (AFM). This provides the typical length scales of the single-stranded DNA, which has a complex secondary structure due to hybridization. The ssDNA blobs give rise to large current blockades. We find a marked increase in the amplitude of the blockage current during translocation with increasing driving voltages. This suggests that the single-stranded DNA is pushed closer to the nanopore at higher voltages, thereby increasingly blocking the ion transport through the pore. A higher applied voltage thus results in a larger access resistance. Furthermore, we demonstrate that the translocation time for single-stranded DNA scales exponentially with voltage, $\tau \sim e^{-V/V_0}$. This can be modeled by a barrier-lowering process, very different than for double-stranded DNA, for which $\tau \sim 1/V$ (cf. ref 7 for example).

Figure 1a sketches the idea of the experiment, depicting a double-stranded DNA molecule with a single-stranded DNA tail. The long dsDNA is captured into the pore and moves to the right, thus applying a force to the hybridized ssDNA blob that subsequently unravels and translocates as well. The experimental setup has been described in detail previously.[23] Briefly, a single nanopore is fabricated in a 20 nm thick, low-stress silicon nitride (SiN) membrane using the focused electron beam of a transmission electron microscope (TEM). The inset of Figure 1 shows a TEM image of a

* To whom correspondence should be addressed. E-mail: c.dekker@tudelft.nl.
Received for review: 01/25/2010
Published on Web: 03/17/2010

© 2010 American Chemical Society

DOI: 10.1021/nl100271c | *Nano Lett.* **2010,** *10,* 1414–1420

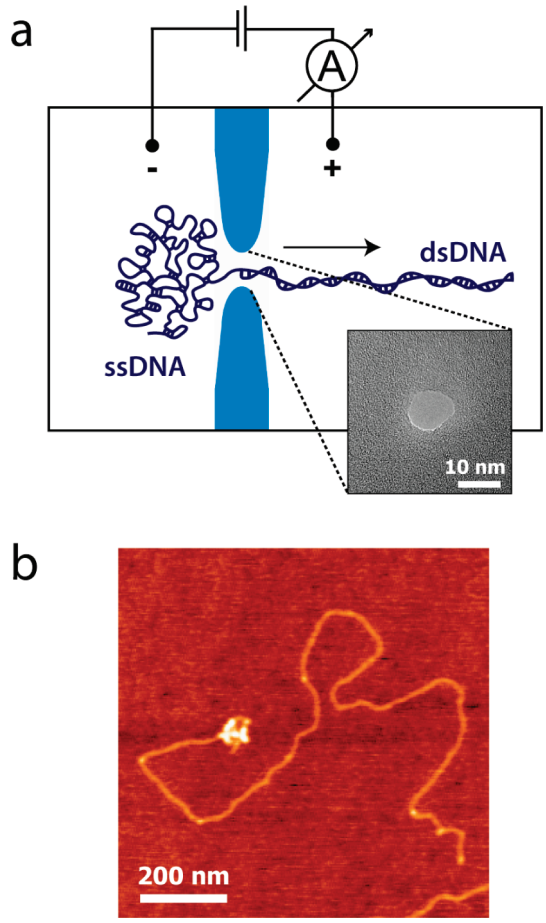

FIGURE 1. (a) Cartoon showing a partly double-stranded and partly single-stranded DNA molecule that is translocated through a nanopore. Intramolecular hybridization causes the single-stranded DNA to have a complex secondary structure that partly has to unravel to fit through the pore. Inset: TEM image of a solid-state nanopore. (b) Atomic force microscope (AFM) image showing a partly double-stranded (the main part) and partly single-stranded (the white blob on the left end of the molecule) DNA molecule that was constructed from double-stranded DNA using ExonucleaseIII.

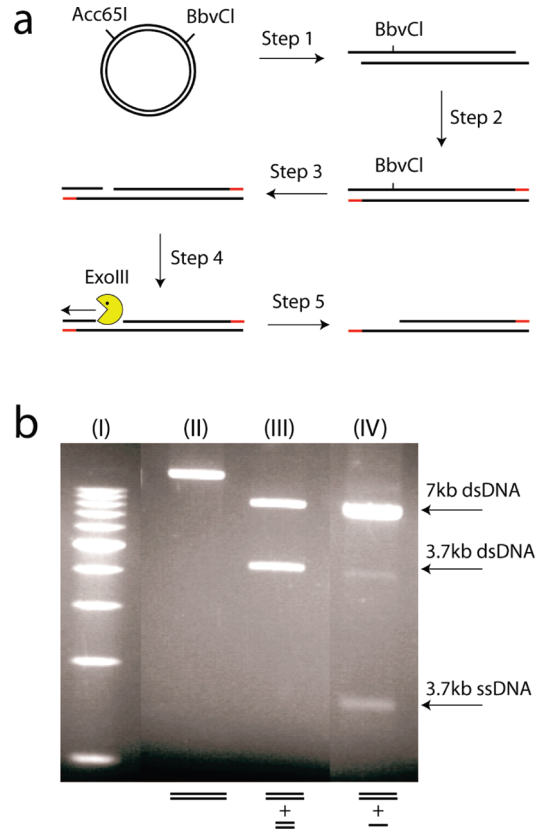

FIGURE 2. (a) Protocol to create double-stranded DNA with a single-stranded tail (details in methods section). (b) Agarose gel showing (I) 1−10 kb dsDNA stepladder, (II) linearized 10.7 kb dsDNA, (III) linearized 10.7 kb dsDNA cut with *Eco*RI, giving bands at 3.7 and at 7 kb, (IV) linearized 10.7 kb dsDNA cut with *Eco*RI after creation of the hybrid DNA. The band at 3.7 kb dsDNA has disappeared, while another band appears near the 1.8 kb dsDNA position. Since ssDNA migrates roughly twice faster than dsDNA, this band is indicative of a ssDNA fragment with a length of about 3.7 kb.

pore that is 9.6 nm in diameter. In this work, we used nanopores of 6.7−9.6 nm in diameter. The membrane is placed between two compartments filled with a monovalent salt solution (1 M KCl) and buffer (10 mM Tris-HCL, pH = 8.0 and 1 mM EDTA). Application of an electric field across the membrane results in an ionic current through the pore, which is temporarily reduced if a molecule passes.

To investigate the translocation and nanopore entrance dynamics of single-stranded versus double-stranded DNA, we constructed long single-stranded tails on double-stranded DNA. Using an Exonuclease III enzyme,[21] we created single-stranded overhangs of three different lengths (3.7, 1.9, and 0.7 kb). Figure 2a shows a schematic of the protocol. First, circular 10.7 kb double-stranded DNA is cut with endonuclease Acc65I to create linear dsDNA (step 1 in Figure 2a). This results in 5′-protruding ends on both sides of the DNA molecule, which are unprotected against *Exo*III. In step 2, the ends are filled in with dNTPαS-nucleotides using Klenow, creating protective blunt ends. Subsequently, a nick is made in the backbone of the DNA-construct using the Nb.BbvCI enzyme (step 3). Finally, the *Exo*III enzyme stepwise removes the nucleotides from the nicking site in 3′ to the 5′ direction (step 4). After this step, some purification and precipitation steps are carried out to purify the construct (step 5). A detailed description of the protocol is found in the methods section.

We study the structure of the molecules using both atomic force microscopy (AFM) and gel electrophoresis. Figure 1b shows an AFM image that displays a molecule with both a single-stranded (flexible) and double-stranded DNA (stiff) part. The single-stranded DNA is highly curled because it has only one backbone with a persistence length of ∼1 nm, significantly smaller than the 50 nm value for dsDNA. Furthermore, the random coil of ssDNA will hybridize to itself. From the AFM data, we found the yield of the desired intact ssDNA−dsDNA construct to be around 84 % ($n = 50$). The remaining part seems to have been broken right at or near the junction, which may be due to the deposition of the molecules onto the mica or the purification. For the intact

© 2010 American Chemical Society

DOI: 10.1021/nl100271c | *Nano Lett.* **2010,** *10,* 1414–1420

molecules, we measured the lengths of the dsDNA parts of the molecules from the AFM images. We find an average length of 6.6 ± 0.7 kb for the dsDNA, in good agreement with the expected length of 10.7−3.7 kb = 7.0 kb (see Supporting Information, Figure 2). From the wormlike-chain (WLC) model, generally used for dsDNA,[24−27] we find a radius of gyration of R_g = 840 nm for this 7 kb dsDNA (see Supporting Information). From AFM image analysis, we estimate the size of the ssDNA coil as well. Taking the average of the major and minor axes of an ellipse fit to the image of the ssDNA, we find an approximate size of 63 ± 4 nm for 3.7 kb ssDNA (n = 8). Following ref 28, which studied the relation between DNA coil size in solution connected to that as imaged by AFM on mica and other substrates (see also Supporting Information), this gives an estimated blob diameter in solution of 45 ± 3 nm. On the basis of the freely jointed chain (FJC) model, which is generally used for ssDNA,[24−27] we estimate a diameter of 80 nm for this length ssDNA (see Supporting Information), that is, a fairly similar size. Note that this model is not taking into account intramolecular hybridization. The effect of hybridization on coil size is a priori not clear because there are two competing effects. Hybridization will make local connections that will compact the blob. However, locally hybridized structures have a much higher stiffness due to the 50-fold increased persistence length of the hybridized ssDNA (dsDNA) over ssDNA, which will tend to increase the blob size.

Additionally, we performed a gel analysis of these ds-ssDNA constructs, as presented in Figure 2c. Lane I is a 1−10 kb dsDNA stepladder. Lane II shows the linearized 10.7 kb dsDNA. This DNA is cut right at the junction using *Eco*RI both before (lane III) and after (lane IV) creation of the hybrid construct. As expected, lane III shows two double-stranded DNA pieces, one at around 7 kbp and one at around 3.7 kbp. When the DNA is cut after the creation of the hybrid ds-ssDNA (lane IV), we see that the band at 3.7 kb has disappeared, while another band appears near the 1.8 kb dsDNA position, indicative of a ssDNA fragment with a length of 3.7 kb.

Next we turn to the nanopore data. We successfully translocated the hybrid ss/ds-DNA constructs through solid-state nanopores with a diameter of about 8 nm. Figure 3a shows an example of a time trace of the ionic current through the pore without DNA in the flow cell. A stable baseline is observed with no spikes in the current. After addition of the ss/ds-DNA construct (indicated by the arrow), spikes are observed in the current trace. We zoom in on two example events in Figure 3b. Two blockade levels can be distinguished. We attribute the lower blockade level to dsDNA and the higher blockade level to ssDNA, based on the following. From a large number of such "events" (defined as such a current spike including the current signal 2 ms before and after the event), we can make a conductance histogram as displayed in Figure 4a. A scatter plot of dwell time versus amplitude is presented in the Supporting Information. Next to the base current peak at zero conductance blockade, two peaks are observed near 2 and 8 nS. Comparison with extensively reported previous data for dsDNA translocation experiments (e.g., ref 4) where blockade values of ∼1−2 nS were found, argues that the lower blockade level at around 2 nS is caused by the dsDNA part of the ss/ds-DNA molecules. We subsequently identify the other peak near 8 nS with the ssDNA part of the molecules.

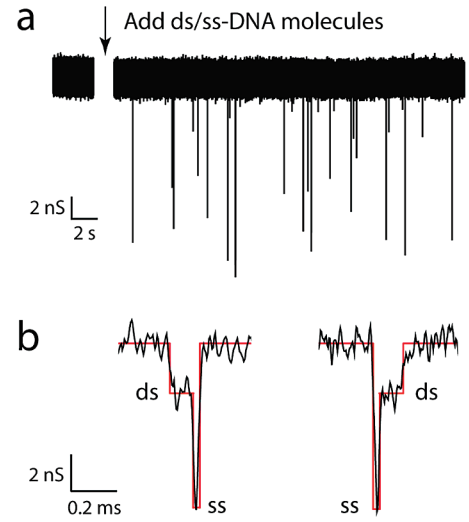

FIGURE 3. (a) Ionic current versus time at an applied voltage of 240 mV. Upon addition of ds/ss-DNA molecules downward spikes appear in the current. The data is recorded at 100 kHz bandwidth and is not filtered additionally. (b) Example traces for translocating ds/ss-DNA molecules. Each translocation event shows two levels, one associated with the dsDNA part, and one with the ssDNA part. We find that in about 80% of the events, the dsDNA enters the pore first, that is, events show the behavior of the trace on the left. The two example traces shown were recorded at 240 mV and filtered at 5 kHz for clarity.

We thus find that the single-stranded DNA induced a very large blockade. This might be surprising in the light of ref 5, where a smaller blockade level of ∼1 nS was found for single-stranded RNA. However, those data were obtained for ssRNA homopolymers such as poly(A), which cannot hybridize as there are no complementary bases available within the molecule. In the current work, however, the ssDNA is a heteropolymer with a random sequence with all nucleotides present, which results in intramolecular hybridization at hundreds of spots; see ref 17 and refs 1−5 therein. This yields a highly connected structure that needs to unravel into much smaller local structures that can each fit through the 8 nm pore in order to translocate the whole construct in a linear fashion. Our nanopores have the shape of an hourglass, and the ssDNA blob will be forced partly into the pore, to the extent allowed by the topology of the interconnected DNA blob, as well as be pressed closely unto the pore entrance due to the electrostatic forces on all DNA segments. This leads to a highly increased conductance blockade. It is interesting to observe that the partial unraveling of the hybridized ssDNA blob indeed occurs under the experimental conditions used, viz. with an applied voltage of ∼100 mV

© 2010 American Chemical Society

DOI: 10.1021/nl100271c | *Nano Lett.* **2010,** *10,* 1414--1420

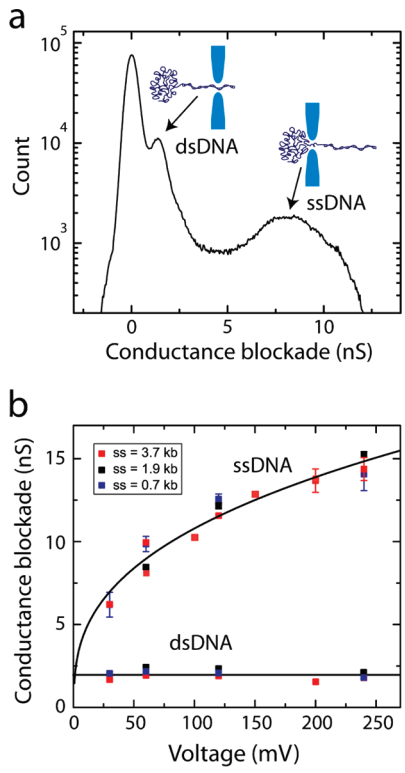

FIGURE 4. (a) Conductance blockade histogram for hybrid 7 kb-dsDNA/ 3.7 kb-ssDNA at 60 mV. Two peaks are visible. We attribute the lower peak to the dsDNA part, and the higher peak to the ssDNA part. (b) Conductance blockade versus applied voltage, for both the double-stranded DNA and single-stranded DNA pieced of hybrid ds/ss DNA molecules for three different lengths of ssDNA (0.7, 1.9, and 3.7 kb). The data show an approximately constant blockade level for dsDNA (2.0 ± 0.3 nS), and a large, voltage-dependent blockade level (~6−15 nS) for ssDNA. The solid lines are fits to the data. For ssDNA we find $\Delta G = aV^b$ with $a = 2.0 \pm 0.3$ nS and $b = 0.37 \pm 0.03$ and with V the voltage in mV. The ssDNA conductance blockade value is, within experimental error, not dependent on the length of the single-stranded part.

that corresponds to forces of tens of piconewtons.[29] Threshold values to mechanically separate two complementary strands of dsDNA have both experimentally[30,31] and theoretically[32] been found to be in the range of approximately 9−20 pN, in accordance with the data presented here.

The voltage dependence of the conductance blockade provides an interesting handle to further distinguish dsDNA and ssDNA. As can be seen from Figure 4b, we find a constant value for the blockade level for dsDNA (2.0 nS) versus voltage, but a highly voltage-dependent value for the blockade level (~6−15 nS) for ssDNA. Interestingly, this result appears to be independent of the length of the ssDNA as the data obtained for different lengths (0.7−3.7 kb) overlap. At higher voltages, dsDNA and ssDNA can be very clearly discriminated. The voltage dependence of the ssDNA blockade level can be understood by considering the access resistance; at higher voltages, the ssDNA blob (which does not fit through the pore without unraveling) is pushed closer to the pore due to the larger electrophoretic forces, thereby increasing the access resistance.[33] We empirically find a dependence $\Delta G = aV^b$, with $a = 2.0 \pm 0.3$ nS and $b = 0.37 \pm 0.03$, where V is the applied voltage in millivolts, independent of the length of the ssDNA within the range probed (0.7−3.7 kb).

For each translocation event of the ssDNA−dsDNA construct, we determined whether the ssDNA or the dsDNA part entered the pore first. We find that the dsDNA entered the pore first in 80% of the events ($N = 11.166$), only then followed by the ssDNA part. In 20% of the events the ssDNA entered first. As an additional experiment, we cut the ssDNA−dsDNA construct right at the junction, using the *Eco*RI restriction enzyme. We then translocated this mixture of both ssDNA and dsDNA (not attached to each other; see Supporting Information Figure 3 for an AFM image), and compared the number of events of dsDNA translocation and ssDNA translocation. This gives similar numbers; 79% of the events are dsDNA translocations, and 21% are ssDNA translocations ($N = 487$). The dsDNA is thus more effective in getting to the pore entrance than ssDNA. While a detailed and quantitative model is lacking at this point, we suggest that the difference in captures rates can be explained simply by the fact that dsDNA has a larger hydrodynamic radius than the ssDNA and thus a larger probability of approaching and entering the pore first.

Additionally, we studied translocation of single-stranded viral DNA isolated from M13mp18 (New England Biolabs). The ssDNA of this M13 lac phage vector is circular and 7.2 kb in length, and has no dsDNA attached to it. AFM imaging of this ssDNA again reveals bloblike structures (see Figure 5a) and taking the average of the minor and major axes of an ellipse fit to the ssDNA images gives a typical diameter of 147 ± 6 nm ($n = 7$). Following ref 28, this gives an estimated typical diameter in solution of 104 ± 4 nm (see also Supporting Information and ref 36). On the basis of the FJC model (thus neglecting intramolecular hybridization) and taking into account that theoretically[34] the relation between circular and linear DNA blob size is given by $\langle R_g^2 \rangle_{circular} = \langle R_g^2 \rangle_{linear}/2$, we estimate a diameter of gyration of 78 nm for this ssDNA, that is, similar to the size as obtained from the AFM data.

Upon translocating the M13mp18 ssDNA through a solid-state nanopore of 7.0 nm in diameter, we observe large peaks with well-defined amplitudes (Figure 5b). Again, the peaks are much larger (about 10-fold) than expected from volume exclusion of one strand of ssDNA. The conductance histogram in Figure 5c shows only one peak, at around 11 nS, next to the base current peak at zero conductance blockade. Compared to the ssDNA−dsDNA (Figure 4a), the peak at around 2 nS is absent. This confirms our claim that the latter peak is caused by dsDNA and that the high-conductance peak is due to ssDNA. The inset of Figure 5d shows the voltage dependence of the ssDNA peak for M13mp18 ssDNA. Again, we find that increased voltage leads to higher blockade values.

© 2010 American Chemical Society

DOI: 10.1021/nl100271c | *Nano Lett.* **2010,** *10,* 1414–1420

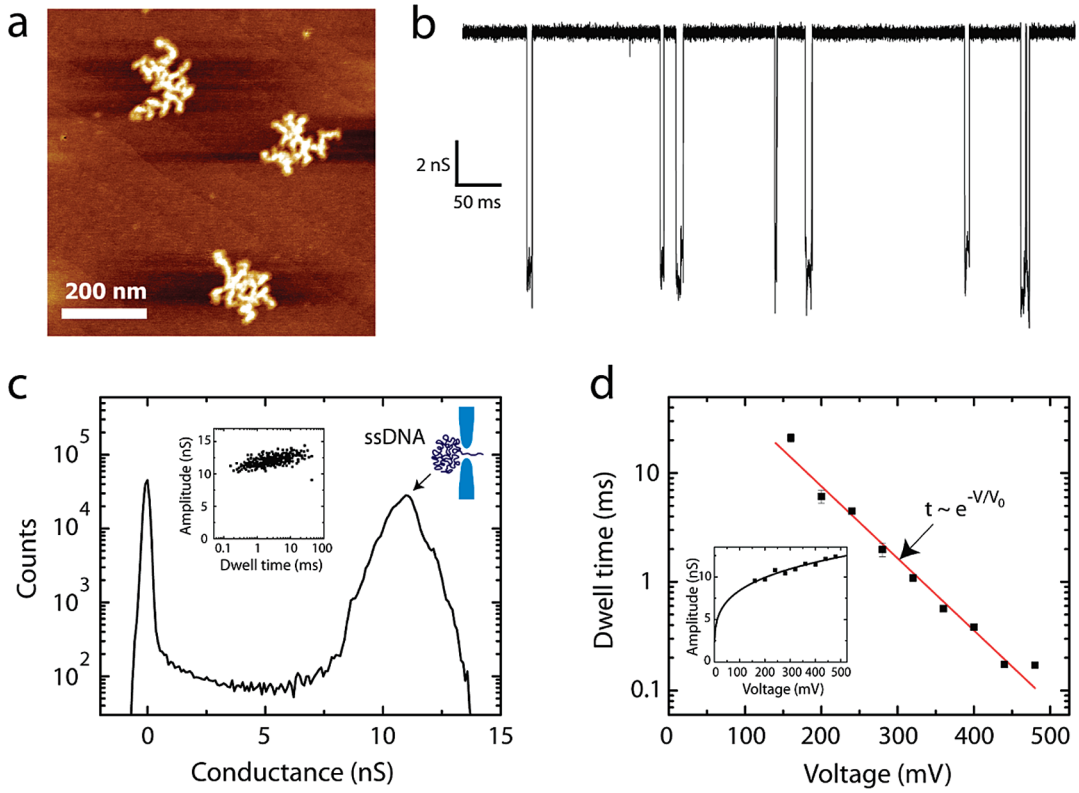

FIGURE 5. (a) AFM image of 7.2 kb M13mp18 ssDNA. Structures of around 150 nm in diameter can be seen to form due to hybridization. (b) Ionic current versus time after addition of this ssDNA at an applied voltage of 240 mV. (c) Conductance histogram, taken at 240 mV. The ssDNA gives a large peak at around 11 nS. Notice that a dsDNA peak is absent. The inset shows a scatter plot at 240 mV. The typical dwell time can be fitted with a log-normal distribution. (d) Dwell time versus voltage for the same ssDNA. We find an exponential voltage dependence. The line is an exponential fit to the data: $\tau = Ae^{-V/V_0}$, where $A = 160 \pm 13$ ms, and $V_0 = 66 \pm 1$ mV. The inset shows ΔG as a function of voltage. The solid line is a fit to the data, with $\Delta G = aV^b$, where $a = 2.8 \pm 0.4$ nS and $b = 0.24 \pm 0.03$ and with V the applied voltage in mV.

It is interesting to see how the dwell times for M13mp18 ssDNA, which can be viewed as the unraveling times, depend on voltage. At each applied voltage, we fit a log-normal distribution to the translocation times (cf. inset to Figure 5c), which yield a typical translocation time at that voltage. The voltage dependence of this dwell time is displayed in Figure 5d. Notably, we find that the ssDNA dwell time depends exponentially on applied voltage, $\tau \sim e^{-V/V_0}$. This is in contrast with what was found for dsDNA, namely $\tau \sim 1/V$ (cf. ref 7). Clearly the physics in both cases is different: in the case of dsDNA, the DNA is simply threaded through the pore, and a larger voltage results in a larger force on the molecule and therefore to a proportionally shorter translocation time. In the case of ssDNA, however, the polymer does not fit through the pore and has to unravel. Presumably in this case, many hydrogen bonds formed during hybridization need to be broken, leading to a large barrier for the molecules to pass through the pore. Apparently the complex unraveling process can be modeled as a barrier-lowering process, $\tau \sim e^{-V/V_0}$, if driven by a force due to an externally applied voltage.

Summing up, with these translocation measurements of both viral single-stranded DNA as well as ssDNA–dsDNA constructs we have explored the distinct behavior of random sequence single-stranded DNA molecules in solid-state nanopores. Surprisingly, we find larger current blockades for ssDNA than for dsDNA, which we account for by an increased resistance due to a large random-coiled blob of hybridized ssDNA at the pore entrance. This blob has to unzip in order to pass through the pore. We find characteristic ssDNA unzipping times at a range of voltages (forces), as well as an exponential dependence on voltage, which is a much stronger dependence than for dsDNA. These findings may be beneficial for nanopore sequencing of ssDNA.

Methods. ***Method for Making Single-Stranded/Double-Stranded DNA Molecules.*** For the construction of single-stranded tails on double-stranded DNA, we developed an enzymatic assay using the 3′ to 5′ exonuclease activity of *Exo*III.[21] This enzyme can initiate on nicks within the DNA, on 3′ recessed ends, blunt ends, and some 3′ protruding ends.[22] In this work, a unique nicking site in the DNA is used for *Exo*III initiation. The DNA ends are protected with special nucleotides that block the initiation of the exonuclease to establish a controlled process with fixed size of the single-stranded tail. The example discussed here, is to make a 7 kb double-stranded fragment with a 3′ protruding single strand tail of 3.7 kb. For this and other fragments made, a 10.7 kb vector is used as starting molecule. This vector has

© 2010 American Chemical Society

DOI: 10.1021/nl100271c | *Nano Lett.* **2010,** *10,* 1414–1420

a unique *BbvC*I nicking site for *Exo*III initiation. First, the vector is linearized with *Acc*65I to created 5′ protruding ends. We then heat inactivated the *Acc*65I, keeping it for 20 min at 65 °C. The ends are then filled-in with modified alpha-thio deoxynucleotides (Jena Bioscience) using exo- Klenow (New England Biolabs) at 37 °C for 25 min. These nucleotides protect the ends for exonuclease initiation by *Exo*III.[22] The restriction and Klenow reactions are performed in NEB3 buffer (New England Biolabs). We then purify using silica membrane columns NucleoSpin Extract II (Macherey Nagel) to change buffers. Subsequently, we nick one strand of the double-stranded molecule with *Nb.BbvC*I in NEB2 and purify again using silica membrane columns to exchange buffers to NEB1 for the *Exo*III reaction. We then determine the concentration of the DNA and use 10 units *Exo*III/μg DNA in NEB1 buffer and incubate for 1 h at 37 °C. Longer incubation times can result in nonspecific exonuclease activity. The DNA is now purified using ethanol precipitation (silica membrane columns could break the single-stranded tails). We found that the processing time is crucial for a successful assay. The various steps are preferably done one right after the other and performed on freshly isolated vector DNA or DNA that is stored in ethanol. Any damage (nicks) on the DNA will result in initiation start sites for *Exo*III on nonspecific locations on the DNA. Variations in length of the single-stranded tail and the size of the double-stranded DNA are controlled by the choice of endonucleases used to linearize the vector. Besides the described 3.7 kb ssDNA fragment, two other fragments were made. Using endonuclease *Xho*I, we created a single-stranded tail of 1944 bp and a double-stranded part of 8.7 kb; using endonuclease *Asc*I, we made a 720 bp single-stranded tail and a double-stranded part of 9.9 kb. Interestingly, variations like dsDNA−ssDNA−dsDNA, or ssDNA−dsDNA−ssDNA are also possible by choosing different nicking and/or cleavage sites (see Supporting Information).

Solid-State Nanopores and AFM Imaging. Solid-state nanopore fabrication starts with the production of 20 nm thin, free-standing SiN membranes through the use of electron-beam lithography and wet etching. In each such membrane, we drill a nanopore of the desired size through the use of a highly focused electron beam in a transmission electron microscope (TEM). Details of the fabrication process are described elsewhere.[23] In this study, we used nanopores of 6.7−9.6 nm in diameter. Directly after drilling, the pores are stored in a solution containing 50% ethanol and 50% ddH_20. Prior to use, the nanopores are treated in an oxygen plasma for 30 s on both sides. Subsequently, the nanopores are mounted in a polyether ether ketone (PEEK) microfluidic flow cell and sealed to liquid compartments on either side of the sample. Measurements are performed in 1 M KCl salt solution containing 10 mM Tris-HCl and 1 mM EDTA at pH 8.0 at room temperature. The high salt is chosen for increased signal-to-noise in the nanopore current signals. Ag/AgCl electrodes are used to detect ionic currents and to apply electric fields. Current traces are measured at 100 kHz bandwidth using a resistive feedback amplifier (Axopatch 200B, Axon Instruments) and digitalized at 500 kHz. When necessary, low-pass filtering is applied. Only pores with minimal low-frequency current noise (<20 pA rms) are used.[35] Tapping-mode atomic force microscopy (AFM) images (Nanoscope IIIa, Digital Instruments, Santa Barbara, CA) were made in air after depositing the DNA molecules in a 20 mM Tris-HCl pH 8.0 and 10 mM $MgCl_2$ buffer on freshly cleaved mica. DNA molecules were tracked using the tracking function in the WSxM software for AFM data analysis.

Acknowledgment. We thank N. H. Dekker, A. R. Hall, M. van den Hout, G. M. Skinner, G. Schneider, M. Y. Wu, and V. Svechnikov for contributions and discussions. This work is supported by the NanoSci-E+ programme and a NWO Spinoza award.

Supporting Information Available. Estimates of radii of gyration for ssDNA and dsDNA from FJC and WLC models, relation between DNA radius of gyration in solution and DNA deposited onto mica, and figures. This material is available free of charge via the Internet at http://pubs.acs.org.

REFERENCES AND NOTES

(1) Dekker, C. Solid-state nanopores. *Nat. Nanotechnol.* **2007**, *2* (4), 209–215.
(2) Howorka, S.; Siwy, Z. Nanopore analytics: sensing of single molecules. *Chem. Soc. Rev.* **2009**, *38* (8), 2360–2384.
(3) Li, J. L.; Gershow, M.; Stein, D.; Brandin, E.; Golovchenko, J. A. DNA molecules and configurations in a solid-state nanopore microscope. *Nat. Mater.* **2003**, *2* (9), 611–615.
(4) Storm, A. J.; et al. Fast DNA translocation through a solid-state nanopore. *Nano Lett.* **2005**, *5* (7), 1193–1197.
(5) Skinner, G. M.; van den Hout, M.; Broekmans, O.; Dekker, C.; Dekker, N. H. Distinguishing single- and double-stranded nucleic acid molecules using solid-state nanopores. *Nano Lett.* **2009**, *9* (8), 2953–2960.
(6) Smeets, R. M. M.; Kowalczyk, S. W.; Hall, A. R.; Dekker, N. H.; Dekker, C. Translocation of RecA-coated double-stranded DNA through solid-state nanopores. *Nano Lett.* **2009**, *9* (9), 3089–3095.
(7) Kowalczyk, S. W.; Hall, A. R.; Dekker, C. Detection of local protein structures along DNA using solid-state nanopores. *Nano Lett.* **2010**, *10* (1), 324–328.
(8) Wanunu, M.; Sutin, J.; Meller, A. DNA profiling using solid-state nanopores: detection of DNA-binding molecules. *Nano Lett.* **2009**, *9* (10), 3498–3502.
(9) Soni, G. V.; Meller, A. Progress toward ultrafast DNA sequencing using solid-state nanopores. *Clin. Chem.* **2007**, *53* (11), 1996–2001.
(10) Branton, D.; et al. The potential and challenges of nanopore sequencing. *Nat. Biotechnol.* **2008**, *26* (10), 1146–1153.
(11) Clarke, J.; Wu, H.-C.; Jayasinghe, L.; Patel, A.; Reid, S.; Bayley, H. Continuous base identification for single-molecule nanopore DNA sequencing. *Nat. Nanotechnol.* **2009**, *4* (4), 265–270.
(12) Kasianowicz, J. J.; Brandin, E.; Branton, D.; Deamer, D. W. Characterization of individual polynucleotide molecules using a membrane channel. *Proc. Natl Acad. Sci. U.S.A.* **1996.**, *93* (24), 13770–13773.
(13) Akeson, M.; Branton, D.; Kasianowicz, J. J.; Brandin, E.; Deamer, D. W. Microsecond time-scale discrimination among polycytidylic acid, polyadenylic acid, and polyuridylic acid as homopolymers or as segments within single RNA molecules. *Biophys. J.* **1999**, *77* (6), 3227–3233.
(14) Meller, A.; Nivon, L.; Brandin, E.; Golovchenko, J.; Branton, D. Rapid nanopore discrimination between single polynucleotide

© 2010 American Chemical Society

DOI: 10.1021/nl100271c | *Nano Lett.* **2010,** *10,* 1414–1420

molecules. *Proc. Natl. Acad. Sci. U.S.A.* **2000**, *97* (3), 1079–1084.
(15) Meller, A.; Nivon, L.; Branton, D. Voltage-driven DNA translocations through a nanopore. *Phys. Rev. Lett.* **2001**, *86* (15), 3435–3438.
(16) Stoddart, D.; Heron, A. J.; Mikhailova, E.; Maglia, G.; Bayley, H. Single-nucleotide discrimination in immobilized DNA oligonucleotides with a biological nanopore. *Proc. Natl Acad. Sci. U.S.A.* **2009**, *106* (19), 7702–7707.
(17) Chen, C. L.; Wang, W. J.; Wang, Z.; Wei, F.; Zhao, X. S. Influence of secondary structure on kinetics and reaction mechanism of DNA hybridization. *Nucleic Acids Res.* **2007**, *35* (9), 2875–2884.
(18) Fologea, D.; et al. Detecting single stranded DNA with a solid state nanopore. *Nano Lett.* **2005**, *5* (10), 1905–1909.
(19) Zhao, Q.; Comer, J.; Dimitrov, V.; Yemenicioglu, S.; Aksimentiev, A.; Timp, G. Stretching and unzipping nucleic acid hairpins using a synthetic nanopore. *Nucleic Acids Res.* **2008**, *36* (5):), 1532–1541.
(20) McNally, B.; Wanunu, M.; Meller, A. Electromechanical unzipping of individual DNA molecules using synthetic sub-2 nm pores. *Nano Lett.* **2008**, *8* (10):), 3418–3422.
(21) Hoheisel, J. D. On the activities of Escherichia-Coli Exonuclease-III. *Anal. Biochem.* **1993**, *209* (2), 238–246, All enzymes used are from New England Biolabs.
(22) Sambrook, J.; Russell, D. W. Mutagenesis. *Molecular Cloning: A Laboratory Manual*; 3rd ed.; Cold Spring Harbor Laboratory Press: Cold Spring Harbor, NY, 1989; Chapter 13.72.
(23) Krapf, D.; et al. Fabrication and characterization of nanopore-based electrodes with radii down to 2 nm. *Nano Lett.* **2006**, *6* (1), 105–109.
(24) Bustamante, C.; Smith, S. B.; Liphardt, J.; Smith, D. Single-molecule studies of DNA mechanics. *Curr. Opin. Struct. Biol.* **2000**, *10* (3), 279–285.
(25) Seol, Y.; Skinner, G. M.; Visscher, K. Elastic properties of a single-stranded charged homopolymeric ribonucleotide. *Phys. Rev. Lett.* **2004**, *93* (11):), 118102.
(26) Tanaka, F. *Introduction to Physical Polymer Science*; Shokabo: Tokyo, 1994.
(27) Rawat, N.; Biswas, P. Size, shape, and flexibility of proteins and DNA. *J. Chem. Phys.* **2009**, *131* (16), 165104.
(28) Rivetti, C.; Guthold, M.; Bustamante, C. Scanning force microscopy of DNA deposited onto mica: Equilibration versus kinetic trapping studied by statistical polymer chain analysis. *J. Mol. Biol.* **1996**, *264* (5), 919–932.
(29) Keyser, U. F.; et al. Direct force measurements on DNA in a solid-state nanopore. *Nat. Phys.* **2006**, *2* (7), 473–477.
(30) Essevaz-Roulet, B.; Bockelmann, U.; Heslot, F. Mechanical separation of the complementary strands of DNA. *Proc. Natl. Acad. Sci. U.S.A.* **1997**, *94* (22), 11935–11940.
(31) Rief, M.; Clausen-Schaumann, H.; Gaub, H. E. Sequence-dependent mechanics of single DNA molecules. *Nat. Struct. Biol.* **1999**, *6* (4), 346–349.
(32) Cocco, S.; Monasson, R.; Marko, J. F. Force and kinetic barriers to unzipping of the DNA double helix. *Proc. Natl. Acad. Sci. U.S.A.* **2001**, *98* (15), 8608–8613.
(33) Aguilella-Arzo, M.; Aguilella, V. M.; Eisenberg, R. S. Computing numerically the access resistance of a pore. *Eur. Biophys. J.* **2005**, *34* (4), 314–322.
(34) Grosberg, A. and Khokhlov, A. *Statistical Physics of Macromolecules*; American Institute of Physics: New York, NY, 1994.
(35) Smeets, R. M. M.; Keyser, U. F.; Dekker, N. H.; Dekker, C. Noise in solid-state nanopores. *Proc. Natl. Acad. Sci. U.S.A.* **2008**, *105* (2), 417–421.
(36) Araki, S.; Nakai, T.; Hizume, K.; Takeyasu, K.; Yoshikawa, K. Hydrodynamic radius of circular DNA is larger than that of linear DNA. *Chem. Phys. Lett.* **2006**, *418*, 255–259.

© 2010 American Chemical Society

DOI: 10.1021/nl100271c | *Nano Lett.* **2010,** *10,* 1414–1420